Title
Deep Vadose Zone Respiration Contributions to Carbon Dioxide Fluxes from a Semiarid Floodplain

Journal
Vadose Zone Journal, 15(7)

ISSN
1539-1663

Authors
Tokunaga, Tetsu K
Kim, Yongman
Conrad, Mark E
et al.

Publication Date
2016-07-01

DOI
10.2136/vzj2016.02.0014

Peer reviewed

Published July 28, 2016

Original Research

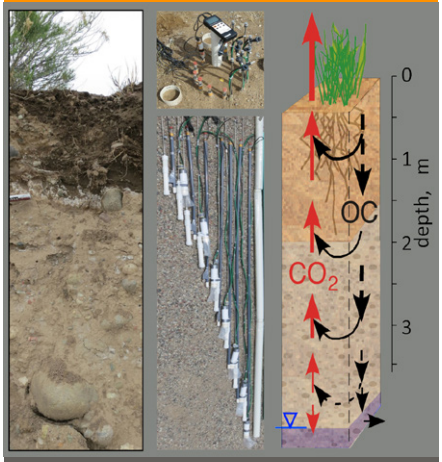

Deep Vadose Zone Respiration Contributions to Carbon Dioxide Fluxes from a Semiarid Floodplain

Tetsu K. Tokunaga,* Yongman Kim, Mark E. Conrad, Markus Bill, Chad Hobson, Kenneth H. Williams, Wenming Dong, Jiamin Wan, Mark J. Robbins, Philip E. Long, Boris Faybishenko, John N. Christensen, Susan S. Hubbard

Although CO_2 fluxes from soils are often assumed to originate within shallow soil horizons (<1-m depth), relatively little is known about respiration rates at greater depths. We compared measured and calculated CO_2 fluxes at the Rifle floodplain along the Colorado River and measured CO_2 production rates of floodplain sediments to determine the relative importance of deeper vadose zone respiration. Calculations based on measured CO_2 gradients and estimated effective diffusion coefficients yielded fluxes that are generally consistent with measurements obtained at the soil surface (326 g C m^{-2} yr^{-1}). Carbon dioxide production from the 2.0- to 3.5-m depth interval was calculated to contribute 17% of the total floodplain respiration, with rates that were larger than some parts of the shallower vadose zone and underlying aquifer. Microbial respiration rates determined from laboratory incubation tests of the sediments support this conclusion. The deeper unsaturated zone typically maintains intermediate water and air saturations, lacks extreme temperatures and salinities, and is annually resupplied with organic carbon from snowmelt-driven recharge and by water table decline. This combination of favorable conditions supports deeper unsaturated zone microbial respiration throughout the year.

Core Ideas

- A significant fraction of CO_2 fluxes from a semiarid floodplain originates from below the root zone.
- Measured and calculated field CO_2 fluxes are consistent.
- Laboratory-measured respiration rates are consistent with field results.

Abbreviations: DOC, dissolved organic carbon; OC, organic carbon.

T.K. Tokunaga, Y. Kim, M.E. Conrad, M. Bill, C. Hobson, K.H. Williams, W. Dong, J. Wan, M.J. Robbins, P.E. Long, B. Faybishenko, J.N. Christensen, and S.S. Hubbard, Earth and Environmental Sciences Area, Lawrence Berkeley National Laboratory, Berkeley, CA 94720. *Corresponding author (tktokunaga@lbl.gov).

Vadose Zone J.
doi:10.2136/vzj2016.02.0014
Received 10 Feb. 2016.
Accepted 18 May 2016.
Supplemental material online.

Vol. 15, Iss. 7, 2016

Fluxes of CO_2 and other gases from soils are important to quantify to understand subsurface feedbacks to the atmosphere and their influences on climate (Pendall et al., 2013; Schlesinger and Andrews, 2000). Most of the CO_2 fluxes leaving the soil surface are commonly attributed to autotrophic (root) and heterotrophic (microbial) respiration occurring at shallow depths (Andrews et al., 1999; Raich and Tufekcioglu, 2000), whereas contributions from below the rhizosphere are less understood. However, the deeper subsurface (>1 m) contains a large inventory of organic carbon (OC), globally estimated to equal or exceed that occurring within the upper 1 m of soils (Batjes, 1996), and supports an abundance of microorganisms (Holden and Fierer, 2005), suggesting that a significant fraction of the CO_2 flux into the atmosphere may be produced below the root zone. Moreover, understanding CO_2 and its isotopic composition in the deep vadose zone is important for determining the age of underlying groundwaters (Bacon and Keller, 1998; Wood et al., 2014).

Unsaturated zone profiles of CO_2 concentration can be combined with estimates of effective gas diffusion coefficients in gradient methods for assessing CO_2 fluxes at the surface as well as within the subsurface (Maier and Schack-Kirchner, 2014; Pingintha et al., 2010). While most studies of subsurface CO_2 profiles and applications of CO_2 gradient analyses are focused on shallow soils, some have investigated considerably deeper systems (Affek et al., 1998; Bacon and Keller, 1998; Davidson and Trumbore, 1995; Garcia et al., 2013; Lewicki et al., 2013; Loisy et al., 2013; Wood et al., 1993). Several of these previous studies have shown the importance of CO_2 production well below the rhizosphere (Affek et al.,

1998; Bacon and Keller, 1998; Wood et al., 1993), even as deep as 110 m below the surface (Walvoord et al., 2005). Very different CO_2 profiles were reported for the two locations investigated by Wood et al. (1993): one in southeastern Washington State, indicative of respiration rates decreasing with depth, and another at Dalmeny (Saskatchewan, Canada), indicative of elevated CO_2 production rates just above the water table. Similarly, CO_2 fluxes from the deeper portion of a 29-m unsaturated zone were calculated to contribute 6.3 g C m^{-2} yr^{-1} and are thought to be sustained by an equivalent flux of dissolved OC supplied through irrigation with sewage effluent (Affek et al., 1998). Recent interest in understanding vadose zone CO_2 profiles has been motivated by the need to detect CO_2 leakage from deep subsurface reservoirs to be used for geologic carbon sequestration (Garcia et al., 2013; Loisy et al., 2013). To our knowledge, longer term measurements needed to examine the persistence of deeper CO_2 production have only been reported for a few sites (Bacon and Keller, 1998; Loisy et al., 2013; Wood et al., 1993). Moreover, although gradient-based studies indicate that deeper profile CO_2 production can be significant, confirmation with direct measurements of deeper sediment respiration rates has not been previously demonstrated. Thus, further investigations of CO_2 production profiles from the soil surface down to the water table are needed, along with analyses of processes responsible for supplying the OC required to sustain respiration in the deeper vadose zone.

Although C exports from floodplains into rivers are well recognized (Noe and Hupp, 2009; Robertson et al., 1999; Shen et al., 2012), transport via groundwater is limited by low flow rates in semiarid regions (Flint and Flint, 2007). Indeed, slower groundwater recharge rates provide more time for microbial degradation of OC and CO_2 release in the vadose zone. While recent research suggests that semiarid region ecosystems exert dominant influences on global trends in CO_2 uptake and interannual variability (Ahlstrom et al., 2015), little is known about the contribution of subsurface C to these net fluxes to the atmosphere. To understand the fate of floodplain subsurface C, quantifying exports via CO_2 fluxes to the atmosphere originating from vadose zone respiration versus exports of dissolved C phases discharged into adjacent rivers (Hotchkiss et al., 2015) is needed. These considerations motivated monitoring surface CO_2 fluxes and vadose zone concentrations of CO_2 along a transect aligned with the general direction of groundwater flow within a semiarid floodplain at Rifle, CO, adjacent to the Colorado River (Fig. 1). Reactive transport modeling predictions of the influences of temperature and water table fluctuations on redox zonation and carbon fluxes through the vadose zone and groundwater of this floodplain were recently presented by Arora et al. (2016). Here we present an analysis of unsaturated zone CO_2 production rates and fluxes based on depth-resolved measurements of CO_2 concentrations combined with field- and laboratory-based estimates of effective diffusion coefficients. These calculated fluxes are compared with surface CO_2 flux measurements. Supporting laboratory measurements included determinations of matric potential-saturation relations and respiration rates in depth-resolved sediment samples.

Site Description

The Rifle floodplain is situated along the Colorado River in western Colorado. The 8.8 ha site was used from 1924 to 1958 for milling of vanadium and uranium ores and disposal of their mill tailings. Removal of the mill tailings and some of the underlying contaminated sediments occurred in 1994 and 1995, and the site was covered with locally derived, uncontaminated, cobbly loam floodplain soil and vegetated with drought-tolerant perennial grasses (primarily tall wheatgrass, *Elymus elongatum*, and western wheatgrass, *Pascopyrum smithii*) by 1996 (U.S. Department of Energy, 1997, 1999). The surficial soil (1.5 to 2.0 m thick at locations instrumented for this study) is underlain by sandy to cobbly Colorado River floodplain alluvium (Shroba and Scott, 1997) interspersed with finer grained and locally organic-rich sediments (Arora et al., 2016; Campbell et al., 2012; Yabusaki et al., 2011). This generally coarse alluvium extends to depths of 6 to 7 m and includes the upper aquifer, with depths to the water table typically ranging from 3.2 to 4 m. The lower boundary of the unconfined upper aquifer consists of relatively low permeability Tertiary Wasatch Formation siltstone.

On average, this semiarid site receives 292 mm of precipitation annually (WRCC, 2014), but monthly average potential evaporation ranges from 0 (December through February) up to 135 mm in July (U.S. Department of Energy, 1999). Monthly precipitation (rain and snow) exceeds potential evapotranspiration from November through March, indicating that the increases in vadose zone water storage commonly occur during these months. While additional infiltration commonly occurs in April and May from precipitation and snowmelt, evapotranspiration from late spring through early fall limits net recharge from the vadose zone into the alluvial aquifer. The combined effects of annually varying weather conditions and microtopographically driven runoff and local ponding have been calculated to limit annual recharge to a range from 0 to at most about 0.1 m yr^{-1}, with an average of only about 0.03 m yr^{-1} (Christensen et al., 2014; Long et al., 2015; Tokunaga et al., 2014). Groundwater flows with reported pore water velocities ranging from 0.1 to 0.8 m d^{-1}, generally south-southwest to the adjacent Colorado River (Anderson et al., 2003; U.S. Department of Energy, 1999; Williams et al., 2011). With goals of understanding water and chemical fluxes through the vadose zone and interactions with underlying groundwater, monitoring and sampling instruments were installed along a 230-m transect aligned with the general groundwater flow direction (Fig. 1).

Numerous borehole-based approaches have been developed for monitoring a variety of properties and processes over widely ranging depths in soils and consolidated rocks (Dahan et al., 2009; Faybishenko, 2000; Hubbell et al., 2004; Levitt et al., 2005; Rimon et al., 2007; Salve, 2011; Sisson et al., 2002; Tokunaga,

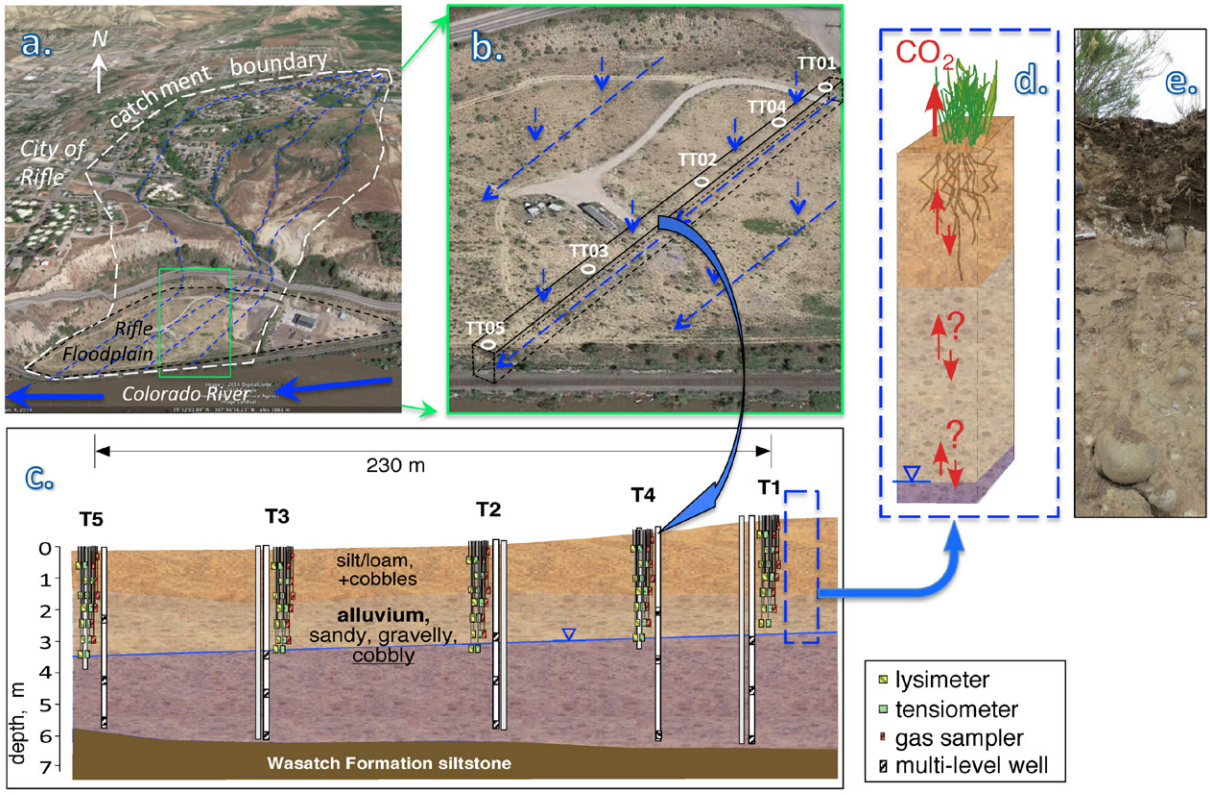

Fig. 1. Rifle floodplain site. (a) Aerial view (Google Earth) of Rifle floodplain, local catchment boundary, and subsurface flow lines estimated from topography. (b) Closer view of the floodplain showing locations of instrumented sites. (c) Cross-section along instrumented sites. (d) Representative vertical profile within which CO_2 fluxes need to be determined. (e) Floodplain soil profile along Colorado River bank, showing gradation to high volumetric fraction of gravels and cobbles at ~1.5-m depth.

1992). However, floodplains in mountainous regions commonly contain cobbles that make borehole instrumentation difficult. To overcome this difficulty, a novel method of borehole instrumentation in sediments containing large cobbles was developed.

Materials and Methods

Borehole Instrumentation

Within the floodplain, five locations were selected for instrumentation along a transect aligned with the general groundwater flow direction (Fig. 1). Three sets of instruments were installed in boreholes in March 2013, with the TT01 instrument suite located furthest north (up-gradient), TT02 within the central floodplain and adjacent to groundwater wells used in studies of microbial communities (Hug et al., 2015), and TT03 further down-gradient and adjacent to well P103 used to investigate naturally reducing zones (Campbell et al., 2012; Janot et al., 2016). The up-gradient TT04 and furthest down-gradient TT05 sites were installed in August 2014. Moderately large diameter access boreholes were drilled through the soil and cobbly alluvium to depths of about 3.5 m by waterless sonic drilling (ASTM, 2004). This method allowed drilling through the coarse sediment that contained some cobbles approaching the 10-inch (0.254 m) diameter of the drill bit and installation of a large number of instruments (Fig. 2). The drill bit was advanced in about 0.6-m increments to recover progressively deeper sediments, typically down to the water table where loss of cohesion prevented deeper drilling and sample recovery. The open, uncased borehole was then accessible for instrumentation. The installations of instruments in 2013 and 2014 were similar, and only the configuration of the more recent installations will be described here. Instrument installation progressed from the deepest interval up to the soil surface. Instrument sets at each depth included a tensiometer (Soil Measurement Systems), matric potential sensor with thermistor (MPS-2, Decagon), soil water sampler (Soilmoisture Equipment Corp. 1900L06, fitted with a no. 10 2-hole rubber stopper connected to a sample extraction tube and another tube for both vacuum application and venting), and gas sampler (constructed from 1-in Schedule 40 PVC pipe, with ~0.08-m sampling length of slotted pipe wrapped with a 30-μm nylon filter cloth). The deepest instrumented depth at each site was 3.50 m beneath the soil surface, with progressively shallower sets of instruments installed at 0.50-m vertical separation distances. Gas samplers were not included at the 3.50-m depths because the water table was often at or above this level.

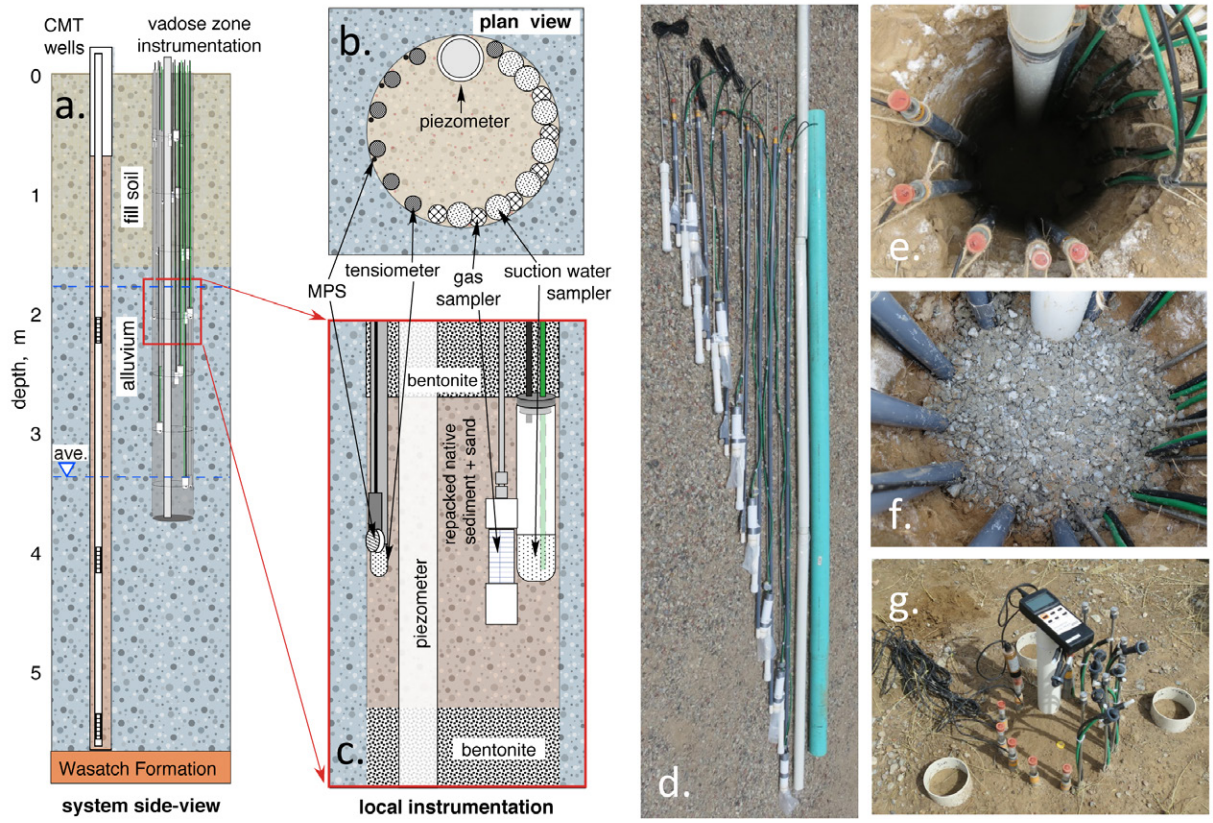

Fig. 2. Installation of borehole instruments. (a) Schematic cross-section of vadose zone instrumentation borehole and multilevel groundwater sampling wells. (b) Plan view of vadose zone instrument distributions along borehole wall. (c) Side view of vadose zone instruments within a given depth. (d) Instruments to be installed in a single borehole (the green pipe was only used to deliver backfill sediments and bentonite to depths greater than 2.5 m). (e) View down partially completed borehole. (f) Near-surface bentonite layer (0.3- to 0.2-m depth). (g) Completed instrumentation, showing tops of tensiometers, soil water samplers, gas samplers, Tensimeter, and several collars for soil surface CO_2 flux measurements.

Sonic drilling allowed recovery of borehole sediments in nearly intact profiles, such that some of this material from each instrumented depth was used for backfilling around instruments. This backfill sediment (excluding larger cobbles) was mixed with 90:100 (150-μm characteristic grain size) silica sand (sand moistened with distilled water to ~0.10 volumetric moisture content prior to mixing with native sediment). The additional silica sand volume fraction within backfill material ranged from ~0.1 to ~0.5 and was needed to compensate for the volume of removed cobbles and sediment retained for laboratory analyses. Each monitoring depth had 0.20 m of native sediment/silica mix backfill below and above the sensor midplane. The 0.10-m intervals between the sediment/silica backfilled zones were filled with 3/8″.bentonite chips prewet to a volumetric moisture content of 0.10 with distilled water. All backfill material was tamped down carefully with a length of 1.5-in PVC pipe fit with a rubber stopper on the bottom end to avoid damaging instruments.

At each monitoring site, a second borehole was drilled down to the contact between the alluvial aquifer and Wasatch Formation siltstone aquitard to allow groundwater sampling. The multilevel groundwater sampling wells (Solinst CMT, 3-Channel System) were assembled to permit sampling at three distinct levels: the deepest region within the aquifer, a zone about 1 m below the typical annual minimum water table depth, and an upper zone that usually remains unsaturated but yields water during the annual peak height of the water table. Depth-distributed thermistors (Campbell Scientific, Model 109SS-L) were installed with the multilevel groundwater sampling wells at sites TT03–05. Although a neutron probe access tube was included in these installations, neutron probe measurements of volumetric water contents were discontinued because of variable influences from backfill material and cobbles.

Tensiometer Measurements

Tensiometer and piezometer measurements were obtained approximately once every 2 wk to determine matric head profiles and to track infiltration fronts and the water table depth. Together with laboratory-determined moisture-characteristic curves, these measurements permitted calculations of air-filled porosity profiles needed for estimating effective diffusion coefficients for CO_2. Calibration of the portable pressure transducer (Tensimeter, Soil Measurement Systems) used to obtain tensiometer readings was initially done in the field with hydrostatic water columns

and reconfirmed annually. Water column head corrections were applied to all field tensiometers readings by using either the height of the visible water surface within the tensiometer top or the water surface calculated from the measured volume of water required to bring the tensiometer water column back up to the viewing region. The tensiometer head correction is referenced to the water level coinciding with the local soil surface, taken as the elevation datum (where the gravitational head $z = 0$). Thus, adding these head corrections (typically within the range of ±0.07 m) to the Tensimeter reading gives the hydraulic head (H), and adding the depth to the tensiometer tip to H gives the matric head (h_m).

Laboratory Analyses for Soil Volumetric Water and Air Contents

Calculations of effective gas diffusion coefficients require estimates of air-fill porosity of the soils and sediments. Because measurements of water retention curves are very time consuming, these were only done for the complete profile at site TT03 and a few selected samples from the other sites within the transect. However, particle-size analyses (Gee and Bauder, 1979) were done for all sites and depths, and similarities in sand–silt–clay fractions were used to assign water retention parameters to the samples lacking measured drainage curves. The pressure plate method (Dane and Hopmans, 2002) was used to determine volumetric water and air contents of soils and sediments down to matric potentials of −100 kPa. The <4.75-mm particle-size fraction of samples (typically at 0.30-m depth intervals) of soils and sediments recovered from borehole drilling were packed inside 5.5-cm-inner-diameter stainless steel rings to a thicknesses of 2.0 cm and presaturated with 20 mM $CaSO_4$ solution. Bulk densities ranged from 1.43 to 1.74 g cm^{-3} for finer to coarser textured samples, respectively. Samples were step-wise drained from −0.1 to −100 kPa on a 1 bar high-flow pressure plate in a 5 bar extractor (Soilmoisture Equipment). To determine saturation-potential relations under drier conditions (beyond the tensiometer range), matric potentials were obtained on some soils by the filter paper method (Scanlon et al., 2002). These results were combined to obtain depth-dependent van Genuchten parameters (van Genuchten, 1980) for the matrix soil and sediment. While the moisture retention relations were determined on the <4.75-mm particle-size fraction, the >4.75-mm grain-size fraction increases with depth in the field site and needs to be considered. Based on field observations (borehole sediment sampling), the volume occupied by the coarse (>4.75 mm) gravels and cobbles was approximated as linearly increasing with depth, from 5% at the soil surface down to 67% of the bulk volume at depths greater than about 1.5 m, and these relative volumes were subtracted from the available porosity.

Carbon Dioxide Flux Measurements

Surface soil CO_2 flux measurements were obtained throughout the year (22 Oct. 2014 to 23 Sept. 2015) with a LI-8100A analyzer (Li-Cor, Lincoln, NE). Most of these measurements were obtained with a 0.10-m-diameter survey chamber (8100–102) cycled through four locations radially distributed around each site (~0.25 m outward from the instrumented borehole), to obtain a morning and a late afternoon–evening CO_2 flux from each quadrant. Given strong temperature dependence of respiration rates, the common localization of higher respiration rates near the soil surface, and daytime heating of the soil surface that is damped within shallow depths, these flux rates exceed those averaged over 24 h. To estimate adjustments needed to represent daily average rates, a separate set of measurements was obtained at several of the sites, with CO_2 fluxes determined at hourly intervals for three consecutive days. These measurements were collected with a 0.20-m-diameter long-term chamber (8100–104, Li-Cor) during the spring (25 Mar. 2015 to 14 Apr. 2015), summer (13 Aug. 2015 to 2 Sept. 2015), and fall (5 Nov. 2015 to 26 Nov. 2015).

Vadose Zone Gas Sampling and Analyses

Soil gas samples were collected at each of the five monitoring sites from October 2014 to September 2015, with greater frequency during summer months because of anticipated higher respiration rates from all ports that were above the water table. In brief, samples were collected with a peristaltic pump connected to the sampling port directly into a 60-mL syringe. After purging one syringe volume, the samples were injected into 60-mL evacuated serum bottles capped with thick blue chlorobutyl septa (Bellco Glass). Gas concentrations were measured with a 2014 Shimadzu gas chromatograph. Using a gas tight syringe, we loaded a sample aliquot of 4.5 mL into a 1-mL stainless steel loop mounted on a 10-port valve (Valco). Carbon dioxide was eluted on a packed HayeSep-D column (4 m by 1/8 in). Carbon dioxide was reduced to CH_4 in a methanizer and quantified with a flame ionization detector.

Carbon Dioxide Diffusion Calculations

Diffusive fluxes were calculated from the product of the effective diffusion coefficient times the measured vertical gradients in CO_2. For this purpose, the water-induced linear reduction model developed by Moldrup et al. (2000) was applied to Marshall's effective diffusion coefficient:

$$D_e = D_o \varepsilon^{2.5} \Phi^{-1} \quad [1]$$

where ε is the air-filled porosity, Φ is the total porosity, and D_o is the diffusion coefficient for CO_2 in the bulk air phase. Recall that Φ is treated as a decreasing depth function (gravel–cobble fraction correction), and ε is calculated from coarse fraction–corrected moisture characteristics and field matric potential measurements. Uncertainties in D_e can become large because of the need to estimate Φ and ε, with the latter variable calculated by approximating the volumetric water content dependence on matric potential as being nonhysteretic. However, by applying best independent estimates of parameters, the general variation of D_e with changes in field moisture regimes is obtainable. The temperature and total pressure dependence of the bulk air phase diffusion coefficient for CO_2 was calculated based on Massman's recommended relation (Massman, 1998):

$$D_o = (1.381 \times 10^{-5}\ m^2\ s^{-1})(101.325\ kPa/P)[T(z,t)/273.15K]^{1.81} \quad [2]$$

where P is the average local atmospheric pressure of 83.7 kPa, and $T(z,t)$ is the time-dependent temperature at a specific depth z (obtained from thermistors at sites TT03 and TT04). It should be noted that at any specific time D_e generally varied with depth, so that values used in calculating Fickian diffusion are harmonic averages of values calculated at adjacent depths. Calculation of CO_2 efflux at the soil surface therefore entailed using harmonic averages of D_e for soil at the 0.50-m depth and at the soil surface (using suitable values of matric head, h_m, at each depth) multiplied by the CO_2 concentration differences (concentration at the 0.50-m depth minus the atmospheric concentration of 0.04 mol %). Lacking measurements of h_m at the soil surface, values of −10 and −100 m were assigned to the soil surface on days associated with moist and dry conditions, respectively. As shown later, calculated D_e are fairly insensitive to reasonable variations of these assumed surface values because water saturations only change gradually with respect to h_m at lower potentials. Much greater uncertainty is encountered when the soil surface is wet. Given the relatively deep position (0.50 m) of the shallowest gas samplers, diffusion-based calculations of CO_2 fluxes are unreliable on days immediately following significant precipitation because steep gradients in water saturation prevent reliable estimates of surface soil D_e. In addition, pulses of highly enhanced respiration rates are commonly observed following precipitation on relatively dry soils (Fierer and Schimel, 2002; Kieft et al., 1987). Thus, on weeks when regional precipitation recorded by the local Rifle weather station (WRCC, 2014) exceeded ASCE evapotranspiration (ASCE-EWRI, 2005), gas sample data were excluded from diffusion calculations.

Laboratory Measurements of Soil–Sediment Respiration Rates

As described below, diffusion-based calculations indicated that significant fractions of CO_2 leaving the soil surface originated from below the root zone (deeper than ~1.5 m). To directly assess the relative importance of deeper subsurface CO_2 production rates and determine the extent to which microbial respiration was responsible, respiration rates (CO_2 production) were measured on sediments collected from different depths at several sites. A comprehensive incubation study is ongoing and will be the focus of a future paper, but a representative subset of results will be described here. Samples were collected from near TT02 and TT04 at depth intervals of 0.0 to 0.3, 0.3 to 1.0, 1.0 to 1.9, 1.9 to 2.6, and 2.6 to 3.5 m below soil surface and immediately sealed in plastic buckets, sieved (4.75 mm), and homogenized in the laboratory. Duplicate 50.00-g samples were placed into 237-mL incubation jars equipped with septum sampling ports (Fierer and Schimel, 2002; Howard and Howard, 1993). After air in the jars was purged with CO_2–free air, the sealed jars were placed in incubators at 25, 21, 21, 17, and 17°C, the approximate depth-dependent average summer subsurface temperatures at the site; field water contents of these samples were 0.10, 0.10, 0.12, 0.13, and 0.15 g g^{-1}, respectively. Incubations were performed on untreated and sterilized (γ-irradiated) soils. Headspace gas samples (3.00 mL) were collected periodically, and CO_2 concentrations were determined with a laboratory infrared gas analyzer (Li-Cor LI-840A). After each sampling event, 3.00 mL of CO_2–free air was replenished into the jar, and measurements continued for 30 d to determine steady state respiration rates.

Results and Discussion

Water Retention Relations

The particle-size fractions and van Genuchten parameters for profiles from the five sites are summarized in Table 1. The field-measured matric head values were used with their site- and depth-specific moisture-characteristic parameters to calculate volumetric water contents, air-filled porosities, and D_e. Representative water retention curves for soils and sediments from TT02 and TT03 are shown in Fig. 3. The data for a typical surface soil from TT02 (Fig. 3a) illustrates the fact that water saturations change gradually over a very wide range of $h_m < -3$ m. Thus, assumed soil surface h_m values of −10 and −100 m for the moist and dry conditions impart relatively small uncertainties in calculated D_e. The large contrast in moisture characteristics of loamy surface soils and deeper coarse alluvium is shown in Fig. 3b.

Hydraulic Head, Matric Head, Volumetric Air Contents, and Gas Diffusion Coefficients

Field-measured hydraulic head (H) values combined with laboratory-measured water retention curves permitted calculation of air-filled porosity profiles and effective diffusion coefficients needed for determining CO_2 fluxes. These measurements and calculations were done for each of the five monitoring sites, but for brevity only results from TT03 will be presented. The H profiles measured at or near times of soil gas sampling (Fig. 4a–4c) are plotted with the local soil surface as the datum for gravitational head ($z = 0.00$ m). Note that the tensiometers in deeper regions of the profile often yield very similar values of H, indicative of near equilibrium with the water table. On each of the H profiles, the tensiometer-inferred water table depth corresponds to its intersection with the dashed diagonal line representing the gravitational head z and was always within ±0.02 m of the measured water table. Despite roughly uniform hydrostatic hydraulic head measured in the deeper portion of the profile, periods of upward flow in response to water table rise, and downward flow in response to water table decline are evident. The H profiles in the upper 2 m clearly show wide variation and reversals of gradients in response to infiltration and evapotranspiration. It should be noted that the uppermost tensiometers were at $z = -0.50$ m, and that values at the soil surface are based on estimates of surface h_m described earlier. The h_m profiles presented in Fig. 4d–4f show wide variations

Table 1. Depth-variation of particle-size fractions, bulk densities, and van Genuchten parameters at the five monitoring sites (excluding estimated volumes of gravel and cobbles).†

Site	Depth	Texture (USDA)			$g + cb$	ρ_b	van Genuchten parameters ($m = 1 - 1/n$)			
		Sand	Silt	Clay			Θ_{sat}	Θ_{res}	α	n
	m	%	%	%		g/cm^3			1/m	
TT-01	0.00–0.50	48	30	22	0.26	1.51	0.43	0.11	2.84	1.42
TT-01	0.50–1.00	34	41	24	0.46	1.47	0.44	0.10	2.35	1.54
TT-01	1.00–1.50	51	34	15	0.67	1.51	0.43	0.13	2.61	1.84
TT-01	1.50–2.00	52	31	18	0.67	1.51	0.43	0.11	2.84	1.42
TT-01	2.00–2.50	46	39	15	0.67	1.51	0.43	0.13	2.61	1.84
TT-01	2.50–3.00	65	26	8	0.67	1.72	0.35	0.09	4.66	1.98
TT02	0.00–0.50	35	42	23	0.26	1.47	0.44	0.10	2.50	1.56
TT02	0.50–1.00	46	36	19	0.46	1.43	0.46	0.05	2.76	1.40
TT02	1.00–1.50	46	33	21	0.67	1.51	0.43	0.11	2.84	1.42
TT02	1.50–2.00	71	20	9	0.67	1.74	0.34	0.13	3.64	2.56
TT02	2.00–2.50	72	17	11	0.67	1.74	0.34	0.13	3.64	2.56
TT02	2.50–3.00	72	17	10	0.67	1.74	0.34	0.13	3.64	2.56
TT03	0.00–0.50	45	33	22	0.26	1.51	0.43	0.11	2.84	1.42
TT03	0.50–1.00	44	44	12	0.46	1.47	0.44	0.10	2.35	1.54
TT03	1.00–1.50	48	34	18	0.67	1.43	0.46	0.05	2.76	1.40
TT03	1.50–2.00	52	32	16	0.67	1.51	0.43	0.13	2.61	1.84
TT03	2.00–2.50	88	10	2	0.67	1.70	0.36	0.11	4.17	2.29
TT03	2.50–3.00	84	9	7	0.67	1.71	0.35	0.10	2.99	2.56
TT04	0.00–0.50	36	39	25	0.26	1.51	0.43	0.11	2.84	1.42
TT04	0.50–1.00	38	42	19	0.46	1.43	0.46	0.05	2.76	1.40
TT04	1.00–1.50	46	39	15	0.67	1.51	0.43	0.13	2.61	1.84
TT04	1.50–2.00	68	22	11	0.67	1.71	0.35	0.10	2.99	2.56
TT04	2.00–2.50	64	23	13	0.67	1.47	0.44	0.10	2.35	1.54
TT04	2.50–3.00	64	23	13	0.67	1.47	0.44	0.10	2.35	1.54
TT05	0.00–0.50	42	49	9	0.26	1.47	0.44	0.10	2.35	1.54
TT05	0.50–1.00	42	49	9	0.46	1.47	0.44	0.10	2.35	1.54
TT05	1.00–1.50	73	20	7	0.67	1.72	0.35	0.09	4.66	1.98
TT05	1.50–2.00	73	20	7	0.67	1.72	0.35	0.09	4.66	1.98
TT05	2.00–2.50	72	21	7	0.67	1.72	0.35	0.09	4.66	1.98
TT05	2.50–3.00	59	17	24	0.67	1.51	0.43	0.11	2.84	1.42

† The depth-dependent estimated volume fractions of gravels and cobbles are noted in the $g + cb$ column.

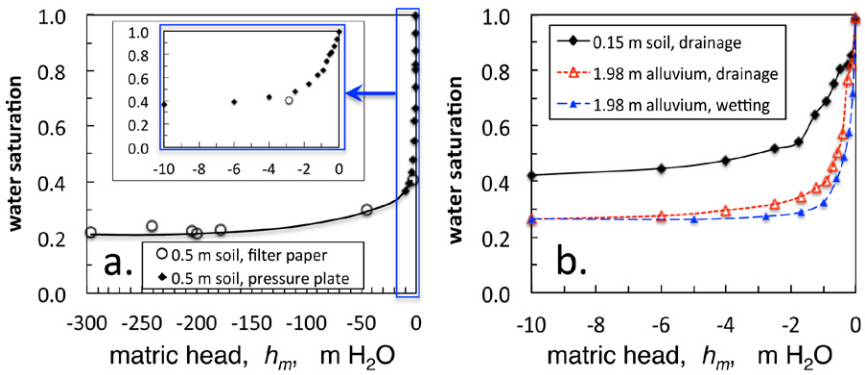

Fig. 3. Representative water retention curves. (a) Drainage (drying) measurements on surface soil from TT02 illustrate the very gradual change in saturation after matric head (h_m) drops below about −3 m H_2O. (b) Contrasting drainage curves representative of loamy surface soils and underlying coarser alluvium.

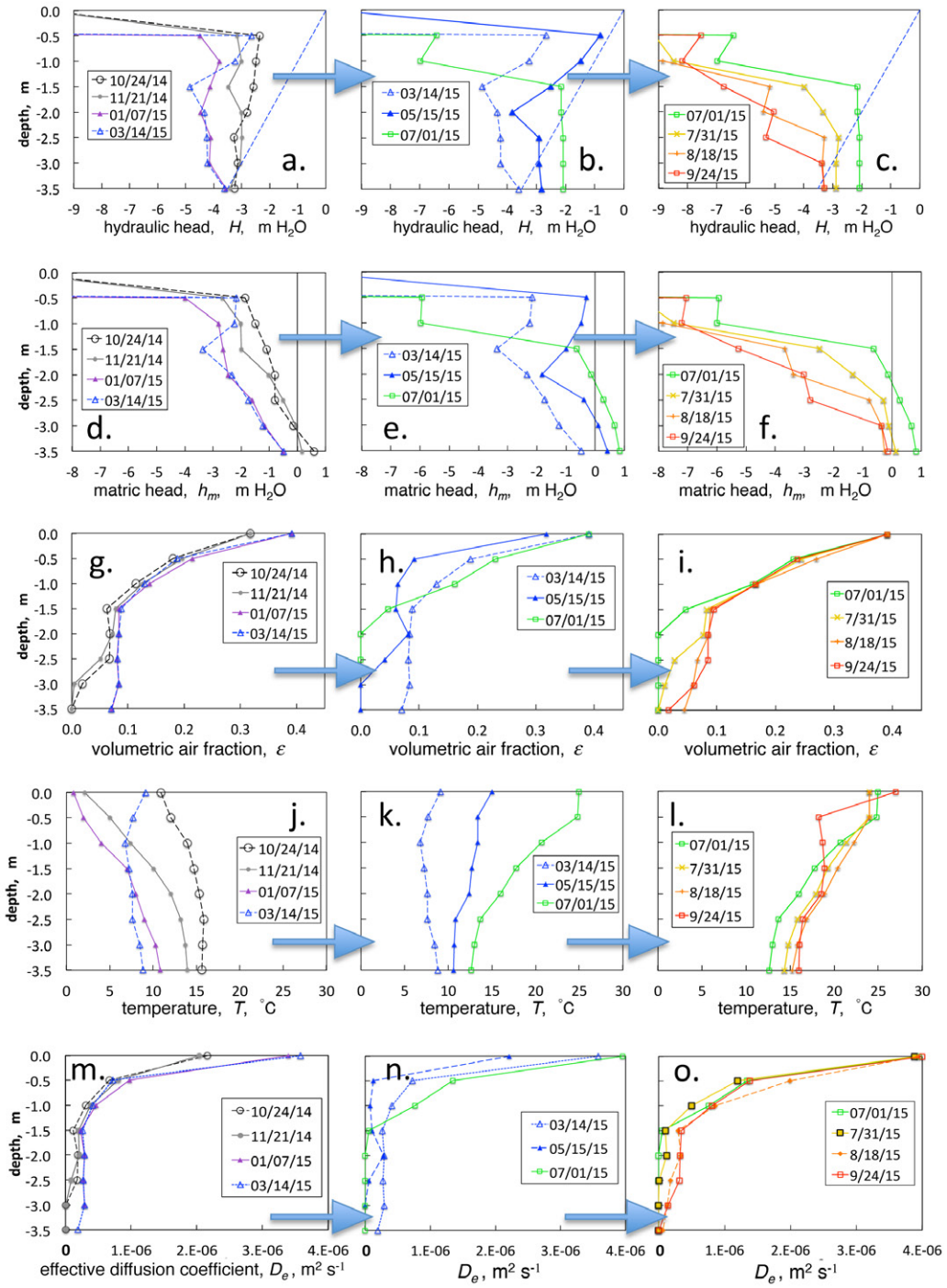

Fig. 4. Seasonal variations in hydraulic and thermal influences on effective CO_2 diffusion coefficient profiles; example from TT03 profile. Hydraulic head (H) profiles (a–c) are used to calculate matric head (h_m) profiles (d–e), which combined with gravels–cobbles-corrected water retention curves yield calculated profiles of volumetric air fractions ε (g–i). Combining profiles of subsurface porosities and temperatures (j–l) yielded depth- and time-dependent D_e (m–o).

and usually more negative values in the upper profile and generally higher values with depth, indicative of prevailing wetter conditions. The h_m profiles were combined with laboratory-measured moisture characteristics to obtain profiles of volumetric air fractions ε, shown in Fig. 4g–4i. In this analysis, ε is set to zero for $h_m \geq 0$ and excluded from diffusion calculations. Although capillary-trapped gas exists below the water table, lack of gas phase continuity with the vadose zone gas phase results in extremely low D_e controlled by the aqueous phase (~10^{-4} that of gas phase diffusion coefficients). The h_m-dependent ε were combined with the depth-dependent estimated total porosities Φ (corrected for gravels and cobbles) and temperature profiles (Fig. 4j–4l) in Eq. [1] and [2] to obtain time-dependent profiles of D_e shown in Fig. 4m–4o.

Carbon Dioxide Flux Measurements

Variation over the monitoring year for measured daytime CO_2 fluxes (averages of morning and afternoon measurements at four locations from each of the five sites), average soil temperature (0.20-m depth), and relative water table elevation are shown in Fig. 5a. While considerable variability exists, the CO_2 fluxes exhibit a clear seasonal pattern: lowest during winter and highest during late spring into summer, reflecting the expected temperature

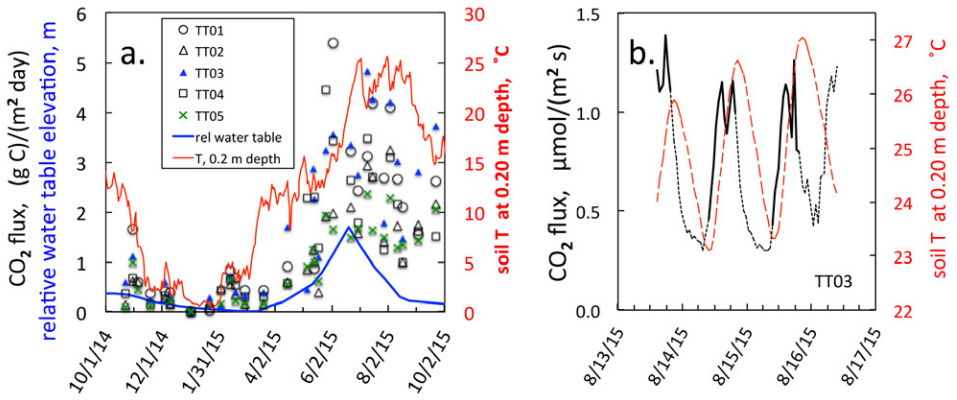

Fig. 5. (a) Time trends in daytime soil surface CO_2 fluxes, near-surface (0.20-m depth) soil temperature, and water table elevation at TT03 relative to its lowest level (3.41 m below soil surface on 13 Mar. 2015). (b) Hourly soil surface CO_2 fluxes (solid black segments of curve indicate daytime 9 AM to 7 PM measurements, and dotted line regions represent overnight measurements) and 0.20-m depth soil temperatures (summer 2015).

dependence (Davidson et al., 1998; Raich and Schlesinger, 1992). The impact of temperature on CO_2 fluxes is further evident in the hourly measurements. The example presented in Fig. 5b includes hourly shallow soil temperatures, showing the daily lag in soil warming at the 0.20-m depth relative to initial morning increases in respiration rates in response to earlier warming at the surface (Loisy et al., 2013). It is clear from these continuous measurements that daytime CO_2 fluxes are generally higher than fluxes averaged over 24-h cycles. Based on 11 different sets of multiday measurements from spring through fall, the CO_2 fluxes collected during the daytime require scaling by a factor of 0.693 (standard deviation of 0.18) to obtain rates suitable for representing a 24-h period. Thus, daytime measured seasonal trends for each site (Fig. 5a) were fit to a third-order polynomial, integrated over 365 d, and multiplied by 0.693, to obtain an average flux of 326 g C m^{-2} yr^{-1} (standard deviation of 87 g C m^{-2} yr^{-1}). This annual flux is within the range of previously reported values for sites in semiarid regions (Table 2).

In addition to the well-known seasonal temperature dependence of CO_2 fluxes, correlation with the yearly rise and fall of the water table at this floodplain site is suggested (Fig. 5a). Because soil gas advection from water table rise and fall must influence CO_2 fluxes, a calculation of its maximum likely contribution was done to assess its significance. Assuming a CO_2 concentration of 1% within the uppermost 0.10-m soil gas phase amounts to 7.2 mmol CO_2 per m^2 of bulk surface soil (84 kPa, 10°C, air porosity of 0.2). Multiplying this near-surface CO_2 concentration by the maximum rate of water table rise of 0.05 m d^{-1} yields a maximum advective flux of 0.04 g C m^{-2} d^{-1}, much smaller than most of the measured surface fluxes. The Peclet number, $Pe = vl/D_e$, where v is the pore gas velocity (at most, 0.05 m d^{-1}) and l is a characteristic length for gas transport at the soil surface (~0.1 m), can also be used to assess the relative importance of advective versus diffusive CO_2 efflux. As seen in Fig. 4, a value of 10^{-6} m^2 s^{-1} provides a reasonable lower limit estimate for D_e, keeping in mind that a lower value confers more importance to advection. Combining these three parameters leads to $Pe \sim 0.06 < < 1$, indicative of only minor advective influence. Thus, we conclude that even during periods with maximum rates of water table rise and fall, CO_2 fluxes at this floodplain site are predominantly diffusive.

Pore Gas Carbon Dioxide Concentrations and Calculated Carbon Dioxide Fluxes

Vadose zone CO_2 concentration profiles at all sites vary seasonally and generally exhibited increases with depth (Fig. 6). Only data from samplers located above the seasonally varying water table (water table depths indicated by horizontal line segments on depth axes) are shown in these plots. Decreases in O_2 concentrations (supplemental material) in close proportion to increases in CO_2 concentrations demonstrated that microbial respiration was far more important than abiotic CO_2 production (Dilly, 2001). Interestingly, CO_2 concentration profiles often exhibit clear maxima in the deeper unsaturated zone, indicating that respiration rates in this zone are high enough to be supplying CO_2 not only to the atmosphere but also into groundwater.

Diffusion of CO_2 from the soil surface into the atmosphere was calculated from each of the concentration profiles by using the gradient method and yielded seasonal variation similar to that of surface flux measurements (Fig. 7a). The average of calculated annual soil surface CO_2 fluxes from the five sites was 317 g C m^{-2} (standard deviation of 117 g C m^{-2}). The linear regression

Table 2. Comparisons among semiarid region annual soil respiration rates.

Environment, location	Mean annual precipitation	CO_2 flux	Source
	mm	g C m^{-2} yr^{-1}	
Cold desert scrub, Utah	244	184	Caldwell et al. (1977)
Cold desert scrub, Utah	244	187	Caldwell et al. (1977)
Creosote desert, New Mexico	211	300	Parker et al. (1983)
Savannah, Australia	850	340	Holt (1987)
Desert scrub, Arizona	310	249	Conant et al. (1998)
Desert scrub transition, Arizona	350	294	Conant et al. (1998)
Steppe, Great Plains, Colorado	320	491	Mosier et al. (2002)
Steppe, natural, Spain	220	416	Rey et al. (2011)
Steppe, degraded, Spain	220	303	Rey et al. (2011)
Semiarid floodplain, Colorado	292	326	this study

between diffusion-based predictions and surface flux measurements (Fig. 7b) yielded a low correlation coefficient (0.542) that was nevertheless highly significant ($P = 0.001$), and the regression slope of about 1.07 (line forced through the origin) indicates general consistency between CO_2 fluxes determined from these two different approached. It should be noted that photodegradation of organic carbon litter at the soil surface can be an important source of CO_2 released to the atmosphere (Cleverly et al., 2013; Rey, 2015; Rutledge et al., 2010). Such releases of CO_2 are not accounted for in the diffusion-based calculated fluxes and are largely missed in the flux chamber measurements.

Although CO_2 concentrations in the deeper soil profiles sometimes exhibited gradients driving fluxes toward groundwater, gradients were predominantly directed upward. For these profiles, the gradient method was also used to calculate upward diffusive CO_2 fluxes originating in the deeper unsaturated zone (below 2.00-m depth at each site), with time trends summarized in Fig. 7c. Despite considerable variability, calculated diffusive fluxes from below 2.00 m averaged 56 g m^{-2} yr^{-1}, amounting to 17% of the measured annual surface flux. Note that the relative importance of deeper unsaturated zone CO_2 fluxes is generally greater during fall–winter (Fig. 7d), when deeper profile is well aerated and temperatures are higher than surface temperatures (Fig. 4j).

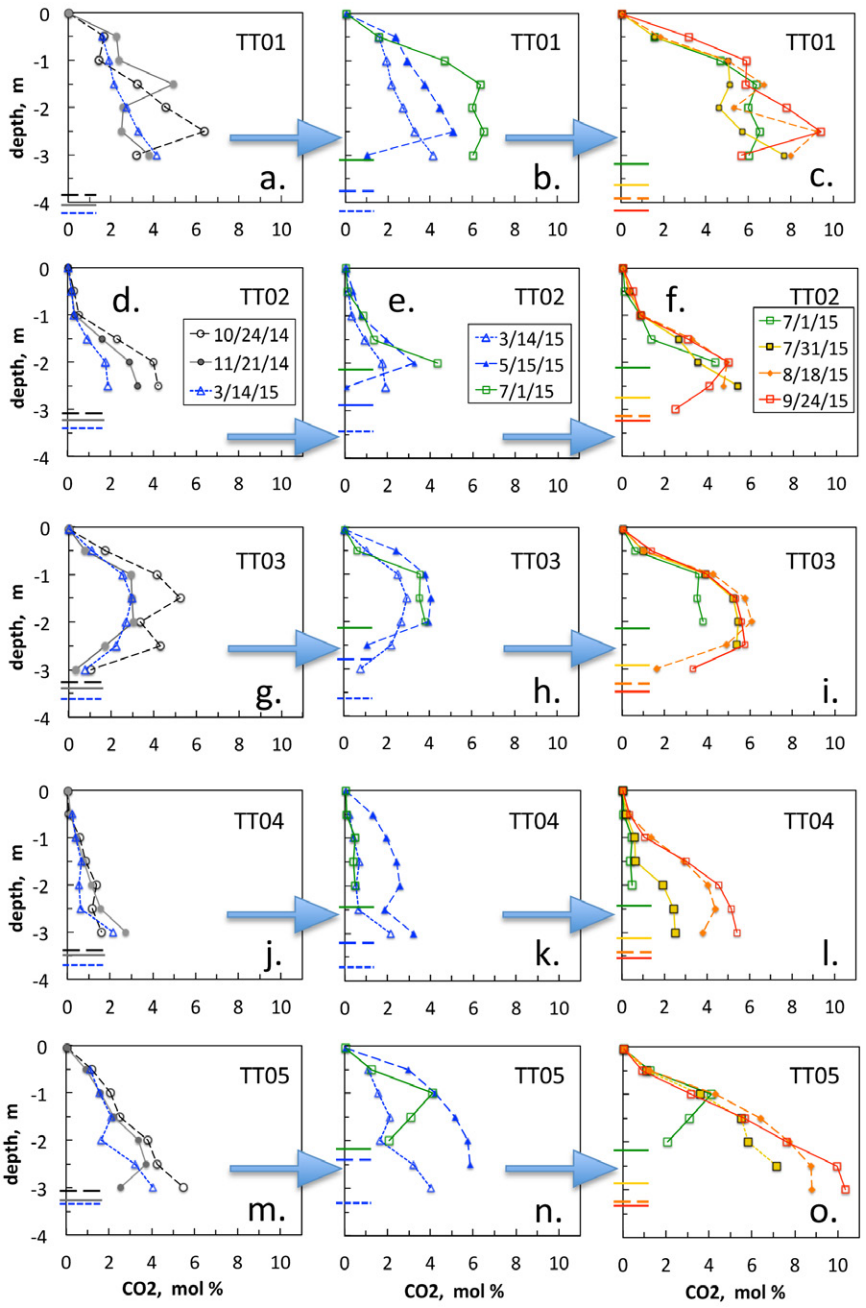

Fig. 6. Depth profiles of unsaturated zone CO_2 concentrations. Seasonal changes in profiles are displayed in left, middle, and right graphs for each of the five sites (sampling dates for all sites are indicated in panels d–f). Horizontal lines along the left axes indicate water table depths at the time of gas sampling.

Before considering the OC flux required to sustain CO_2 production in the deeper vadose zone, it should be mentioned that calcite precipitation releases CO_2 as well. This abiotic reaction explains low rates of CO_2 production (~1 g m^2 yr^{-1}) in the deep vadose zone of the Armagosa Desert (Walvoord et al., 2005). However, the measured decreased O_2 concentrations in slightly greater proportion (1.36 mol mol^{-1}) to increased CO_2 concentrations of vadose zone gases (Supplement) points to the dominance of microbial degradation of OC in the Rifle floodplain. Because roots were not observed below depths of 1.5 m, sustainability of respiration rates in the deeper vadose zone (taken here as the 2.0- to 3.5-m depth interval) requires periodic supply of OC from the overlying surface soil or from groundwater. The latter source was considered minor because of the low dissolved organic carbon (DOC) concentration of about 0.3 mM. On the other hand, DOC concentrations recovered from shallower soil water samplers at depths of 0.5, 1.0, and 1.5 m are typically ~5 ± 2 mM, indicating that the rhizosphere sustains high concentrations of mobile organic carbon (W. Dong et al., unpublished data, 2016). Tensiometer and piezometer measurements indicate that spring infiltration combined with summer water table decline are effective in displacing shallow pore waters into the deeper vadose zone. Infiltration during spring due to increased precipitation and snowmelt during a period with low evapotranspiration drives shallower pore water down to depths between 1.5 and 2.0 m below the soil surface (Fig. 4b). The rapid

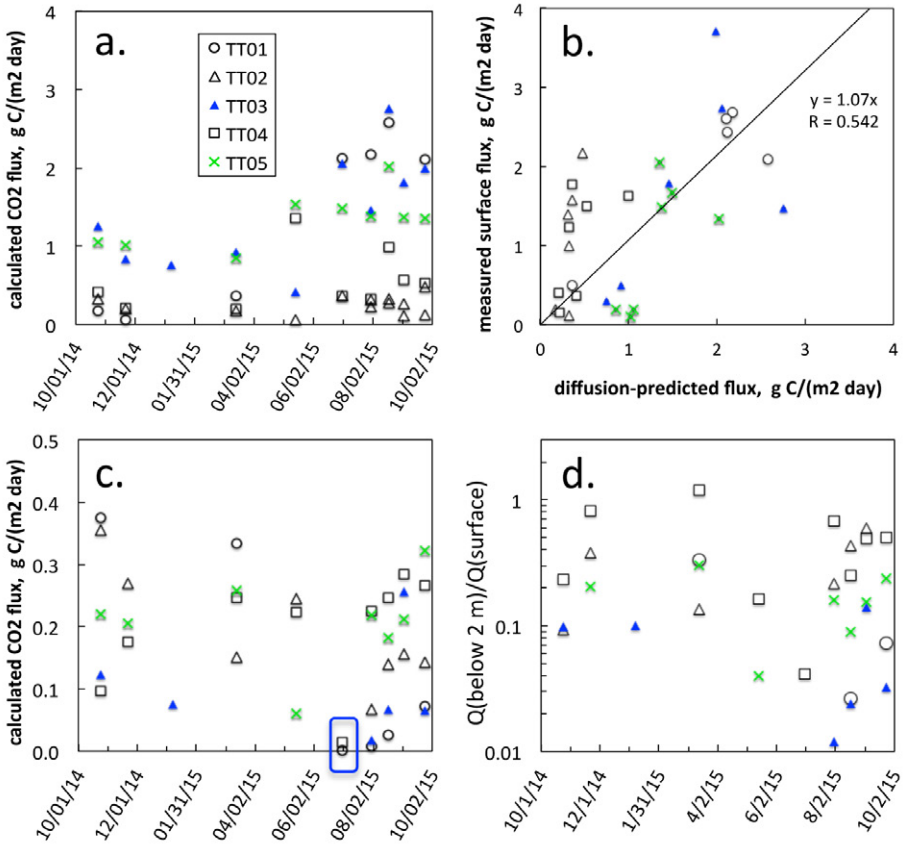

Fig. 7. Diffusive CO_2 fluxes estimated from concentration gradients. (a) Calculated variations in fluxes at the soil surface over a 1-yr time interval. (b) Comparisons between diffusion-based CO_2 fluxes and surface measurements. (c) Calculated CO_2 fluxes at 2.0 m depth over time. Very low flux values within the blue frame at 1 July 2015 are from seasonally submerged deeper profiles where the water table recently receded. (d) Ratios of calculated diffusive CO_2 fluxes originating from below 2.00 m depth relative to the soil surface.

variation in water table elevation of about 1.8 m closely tracks the annual spring to early summer variation in the Colorado River stage caused by snowmelt and runoff from the Rocky Mountains. Downward water displacement is stalled by the sharp annual water table rise (May), and then resumed with decline of the water table (June–August) (Fig. 4b–4c). Thus, shallow rhizosphere pore waters drain into the deeper vadose zone on an annual cycle, yet net groundwater recharge is limited by summer evapotranspiration and the seasonal rise in the water table. The amount of OC transported downward was estimated as the product of a representative rhizosphere DOC concentration of 5 mM, average spring season volumetric water content of 0.29, and 1.8-m water table decline, yielding 31 g C m^{-2} yr^{-1}. This estimated advective DOC flux into the deeper vadose zone accounts for 55% of the calculated annual deeper profile respiration.

Smaller sources of OC for respiration in the deeper vadose zone include advection of colloidal OC excluded from sampling through ~1-μm pores of soil water samplers (Toosi et al., 2014; Zsolnay, 2003), diffusive supply of DOC from overlying sediments, and adsorbed and solid phase OC in the sediments. Although the total organic carbon concentrations in the deeper vadose zone of about 3 g kg^{-1} likely contribute to some of the deeper profile respiration, resupply of OC is clearly needed to sustain respiration in deeper sediments. While balance between transport of OC from the soil surface and its oxidation at depth has been invoked in previous studies (Affek et al., 1998; Wood et al., 1993), the dynamics of such replenishment for supporting deeper profile respiration rates are complex. In addition to uncertainties in recharge rates (especially in semiarid regions), the deeper OC is generally less bioavailable (Kaiser and Kalbitz, 2012; Schwesig et al., 2003). Thus, improvements are needed in understanding deeper profile respiration rates, their associated required DOC influxes, and C transport across the capillary fringe and groundwater.

Laboratory Measurements of Depth-Dependent Carbon Dioxide Production Rates

Trends in gas analyses from the incubated soils exhibited initial rapid increases in CO_2 concentrations that persisted for only a few days, followed by slower but nearly constant and depth-specific production rates in unsterilized samples (Fig. 8). Sterilized samples also exhibited the short initial rapid increases in CO_2 concentrations attributable to recovery of residual unpurged CO_2 and degassing from the aqueous phase, followed by prolonged steady levels showing no further production. Thus, the steady rates of CO_2 production measured in all of the unsterilized samples demonstrate the importance of microbial respiration throughout the unsaturated zone. Moreover, the higher respiration rate measured on the 1.9- to 2.6-m depth interval relative to adjacent shallower and deeper sediments is consistent with calculations based on measured CO_2 concentration profiles and estimated D_e. The lower (more negative) matric and solute potentials associated with the adjacent shallower sediment and lower available organic C in the deeper sediments are factors favoring locally elevated respiration rates in the 1.9- to 2.6-m depth interval. After scaling down respiration rates to account for coarse fraction gravels and cobbles (assumed to have negligible respiration) as described earlier, a profile-integrated respiration rate of 0.96 g C m^{-2} d^{-1} was obtained. Although this value is only about half the typical summer respiration rate measured at the Rifle floodplain, it should be noted that the laboratory measurements do not include root respiration. The contribution of root respiration to total soil respiration has been reported to range from at least 24% (Raich

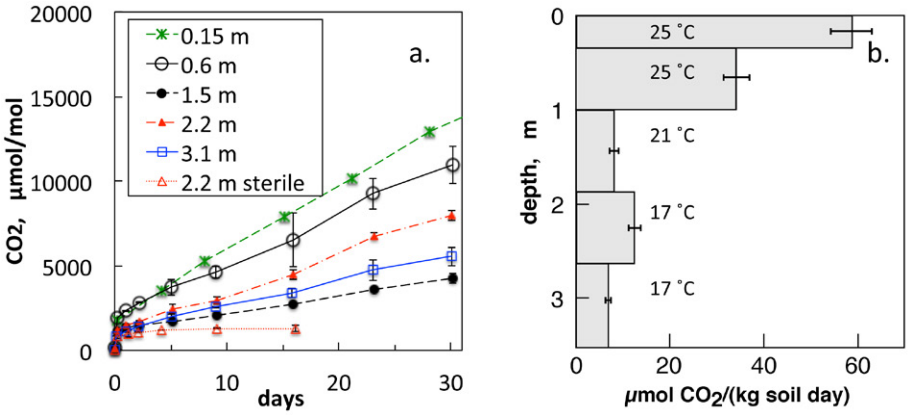

Fig. 8. Carbon dioxide production rates measured in laboratory-incubated sediments. (a) Carbon dioxide concentrations in the headspace of incubation jars containing sediments from different depths in the unsaturated zone. Only one of the sterilized sediment samples is shown. (b) Depth profiles of CO_2 production rates, corrected for approximate fractions of coarse fraction (gravel and cobble). Incubation temperatures representative of depth-dependent average summer temperatures are indicated on the bars.

and Schlesinger, 1992) to as much as 55% (Andrews et al., 1999). More pertinent to our study, the respiration rates obtained on the deeper sediments (1.9 to 3.5 m) are equivalent to 0.23 g C m^{-2} d^{-1}, a value within the range obtained by the gradient method calculations at the 2.0-m depth for summer conditions at the field sites. Thus, the incubation results demonstrate the importance of subrhizosphere CO_2 production.

Conclusions

Microbial respiration in the deeper vadose zone (below 2.0 m) was found to contribute a significant fraction of the annual CO_2 flux to the atmosphere from a semiarid region floodplain at Rifle, CO. Year-long measurements of soil surface CO_2 fluxes and diffusion calculations based on soil CO_2 concentration gradients at five monitoring sites yielded similar rates of 326 and 317 g C m^{-2} yr^{-1}, respectively, and similar seasonal variations. The annual respiration contribution from vadose zone sediments deeper than 2 m was about 17% of the total soil surface flux. A laboratory incubation study conducted under summer conditions provided independent support for elevated respiration rates in the deeper vadose zone. The unexpectedly large and relatively steady release of CO_2 in the deeper vadose zone is attributed to nearly year-round favorable moisture, temperature, and oxygen levels, and an annual supply of soil organic carbon transported through snowmelt-driven recharge and water table decline. Moreover, efficient oxidative depletion of OC in the deeper vadose zone substantially limits OC transport from its rhizosphere origin into groundwater, thereby amplifying the role of soil surface CO_2 fluxes as the dominant C export pathway in this semiarid floodplain.

Supplementary Material

Oxygen concentrations were measured on two sets of samples, 3 and 24 Sept. 2015 (5 sites each). Plots of O_2 concentrations with respect to their associated CO_2 concentrations show that oxygen depletion largely accounts for increases in CO_2 concentrations.

Acknowledgments

This work was conducted as part of the Genomes to Watershed Scientific Focus Area at Lawrence Berkeley National Laboratory, and was supported by the U.S. Department of Energy (DOE) Subsurface Biogeochemical Research Program, DOE Office of Science, Office of Biological and Environmental Research, under Contract Number DE-AC02-05CH11231. The invaluable support provided by the late Richard Dayvault of S.M. Stoller Corporation is gratefully acknowledged and remembered. We also thank Ben Potter (Stoller Corp., thermistor datalogging), Roelof Versteeg (Subsurface Insights, thermistor data), Rocky Cain (Cascade Drilling), and Craig Goodknight (Stoller, sediment logging). We thank the anonymous reviewers and Associate Editor Jörg Bachmann for their very helpful comments.

References

Affek, H.P., D. Ronen, and D. Yakir. 1998. Prediction of CO_2 in the capillary fringe of a deep phreatic aquifer. Water Resour. Res. 34:989–996. doi:10.1029/98WR00095

Ahlstrom, A., M.R. Raupach, G. Schurgers, B. Smith, A. Arneth, M. Jung, M. Reichstein, J.G. Canadell, P. Friedlingstein, A.K. Jain, E. Kato, B. Poulter, S. Sitch, B.D. Stocker, N. Viovy, Y.P. Wang, A. Wiltshire, S. Zaehle, and N. Zeng. 2015. The dominant role of semi-arid ecosystems in the trend and variability of the land CO_2 sink. Science 348:895–899. doi:10.1126/science.aaa1668

Anderson, R.T., H.A. Vrionis, I. Ortiz-Bernad, C.T. Resch, P.E. Long, R. Dayvault, K. Karp, S. Marutzky, D.R. Metzler, A. Peacock, D.C. White, M. Lowe, and D.R. Lovley. 2003. Stimulating the in situ activity of *Geobacter* species to remove uranium from the groundwater of a uranium-contaminated aquifer. Appl. Environ. Microbiol. 69:5884–5891. doi:10.1128/AEM.69.10.5884-5891.2003

Andrews, J.A., K.G. Harrison, R. Matamala, and W.H. Schlesinger. 1999. Separation of root respiration from total soil respiration using carbon-13 labeling during Free-Air Carbon Dioxide Enrichment (FACE). Soil Sci. Soc. Am. J. 63:1429–1435. doi:10.2136/sssaj1999.6351429x

Arora, B., N.F. Spycher, C.I. Steefel, S. Molins, M. Bill, M.E. Conrad, W.M. Dong, B. Faybishenko, T.K. Tokunaga, J.M. Wan, K.H. Williams, and S.B. Yabusaki. 2016. Influence of hydrological, biogeochemical and temperature transients on subsurface carbon fluxes in a flood plain environment. Biogeochemistry 127:367–396. doi:10.1007/s10533-016-0186-8

ASCE-EWRI. 2005. The ASCE standardized reference evapotranspiration equation. Environmental and Water Resources Institute, American Society of Civil Engineers, Reston, VA.

ASTM. 2004. Standard practices for sonic drilling for site characterization and installation of subsurface monitoring devices. ASTM D6914-04. ASTM International, West Conshohocken, PA.

Bacon, D.H., and C.K. Keller. 1998. Carbon dioxide respiration in the deep vadose zone: Implications for groundwater age dating. Water Resour. Res. 34:3069–3077. doi:10.1029/98WR02045

Batjes, N.H. 1996. Total carbon and nitrogen in the soils of the world. Eur. J. Soil Sci. 47:151–163. doi:10.1111/j.1365-2389.1996.tb01386.x

Caldwell, M.M., R.S. White, R.T. Moore, and L.B. Camp. 1977. Carbon balance, productivity, and water-use of cold-winter desert shrub communities dominated by C3 and C4 species. Oecologia 29:275–300. doi:10.1007/BF00345803

Campbell, K.M., R.K. Kukkadapu, N.P. Qafoku, A.D. Peacock, E. Lesher, K.H. Williams, J.R. Bargar, M.J. Wilkins, L. Figueroa, J. Ranville, J.A. Davis, and P.E. Long. 2012. Geochemical, mineralogical and microbiological characteristics of sediment from a naturally reduced zone in a uranium-contaminated aquifer. Appl. Geochem. 27:1499–1511. doi:10.1016/j.apgeochem.2012.04.013

Christensen, J.N., A.E. Shiel, M.E. Conrad, K.H. Williams, W. Dong, T.K. Tokunaga, J. Wan, P.E. Long, and S.S. Hubbard. 2014. Uranium and strontium isotopic study of the hydrology of the alluvial aquifer at the Rifle former U mine tailings site, Colorado. In: American Geophysical Union Fall Meeting. American Geophysical Union, San Francisco, CA.

Cleverly, J., N. Boulain, R. Villalobos-Vega, N. Grant, R. Faux, C. Wood, P.G. Cook, Q. Yu, A. Leigh, and D. Eamus. 2013. Dynamics of component carbon fluxes in a semi-arid Acacia woodland, central Australia. J. Geophys. Res. Biogeosci. 118:1168–1185. doi:10.1002/jgrg.20101

Conant, R.T., J.M. Klopatek, R.C. Malin, and C.C. Klopatek. 1998. Carbon pools and fluxes along an environmental gradient in northern Arizona. Biogeochemistry 43:43–61. doi:10.1023/A:1006004110637

Dahan, O., R. Talby, Y. Yechieli, E. Adar, N. Lazarovitch, and Y. Enzel. 2009. In situ monitoring of water percolation and solute transport using a vadose zone monitoring system. Vadose Zone J. 8:916–925. doi:10.2136/vzj2008.0134

Dane, J.H., and J.W. Hopmans. 2002. Pressure plate extractor. In: J.H. Dane and G.C. Topp, editors, Methods of soil analysis, Part 4, Physical Methods. Soil Science Society America, Madison, WI. p. 688–690.

Davidson, E.A., E. Belk, and R.D. Boone. 1998. Soil water content and temperature as independent or confounded factors controlling soil respiration in a temperate mixed hardwood forest. Glob. Change Biol. 4:217–227. doi:10.1046/j.1365-2486.1998.00128.x

Davidson, E.A., and S.E. Trumbore. 1995. Gas diffusivity and production of CO_2 in deep soils of the eastern Amazon. Tellus B Chem. Phys. Meterol. 47:550–565. doi:10.1034/j.1600-0889.47.issue5.3.x

Dilly, O. 2001. Microbial respiratory quotient during basal metabolism and after glucose amendment in soils and litter. Soil Biol. Biochem. 33:117–127. doi:10.1016/S0038-0717(00)00123-1

Faybishenko, B. 2000. Tensiometer for shallow and deep measurements of water pressure in vadose zone and groundwater. Soil Sci. 165:473–482. doi:10.1097/00010694-200006000-00003

Fierer, N., and J.P. Schimel. 2002. Effects of drying-rewetting frequency on soil carbon and nitrogen transformations. Soil Biol. Biochem. 34:777–787. doi:10.1016/S0038-0717(02)00007-X

Flint, L.E., and A.L. Flint. 2007. Regional analysis of ground-water recharge. In: D.A. Stonestrom, J. Constantz, T.P.A. Ferré, and S.A. Leake, editors, Ground-water recharge in the arid and semiarid southwestern United States. U.S. Geological Survey, Denver, CO. p. 29–59.

Garcia, B., P. Delaplace, V. Rouchon, C. Magnier, C. Loisy, G. Cohen, C. Laveuf, O. Le Roux, and A. Cerepi. 2013. The CO_2–vadose project: Numerical modeling to perform a geochemical monitoring methodology and baseline performance assessment for various geochemical variables (gas flux, gas composition, stable isotopes and noble gases) in the carbonate vadose zone. Int. J. Greenh. Gas Control 14:247–258. doi:10.1016/j.ijggc.2013.01.029

Gee, G.W., and J.W. Bauder. 1979. Particle-size analysis by hydrometer: A simplified method for routine textural analysis and a sensitivity test of measurement parameters. Soil Sci. Soc. Am. J. 43:1004–1007. doi:10.2136/sssaj1979.03615995004300050038x

Holden, P.A., and N. Fierer. 2005. Microbial processes in the vadose zone. Vadose Zone J. 4:1–21. doi:10.2113/4.1.1

Holt, J.A. 1987. Carbon mineralization in semiarid northeastern Australia: The role of termites. J. Trop. Ecol. 3:255–263. doi:10.1017/S0266467400002121

Hotchkiss, E.R., R.O. Hall, R.A. Sponseller, D. Butman, J. Klaminder, H. Laudon, M. Rosvall, and J. Karlsson. 2015. Sources of and processes controlling CO_2 emissions change with the size of streams and rivers. Nat. Geosci. 8:696. doi:10.1038/ngeo2507

Howard, D.M., and P.J.A. Howard. 1993. Relationships between CO_2 evolution, moisture-content and temperature for a range of soil types. Soil Biol. Biochem. 25:1537–1546. doi:10.1016/0038-0717(93)90008-Y

Hubbell, J.M., M.J. Nicholl, J.B. Sisson, and D.L. McElroy. 2004. Application of a Darcian approach to estimate liquid flux in a deep vadose zone. Vadose Zone J. 3:560–569. doi:10.2113/3.2.560

Hug, L.A., B.C. Thomas, T.C. Brown, K.R. Frischkorn, K.H. Williams, S.G. Tringe, and J.F. Banfield. 2015. Aquifer environment selects for microbial species cohorts in sediment and groundwater. ISME J. 9:1846–1856. doi:10.1038/ismej.2015.2

Janot, N., J.S.L. Pacheco, D.Q. Pham, T.M. O'Brien, D. Hausladen, V. Noel, F. Lallier, K. Maher, S. Fendorf, K.H. Williams, P.E. Long, and J.R. Bargar. 2016. Physico-chemical heterogeneity of organic-rich sediments in the Rifle aquifer, CO: Impact on uranium biogeochemistry. Environ. Sci. Technol. 50:46–53. doi:10.1021/acs.est.5b03208

Kaiser, K., and K. Kalbitz. 2012. Cycling downwards: Dissolved organic matter in soils. Soil Biol. Biochem. 52:29–32. doi:10.1016/j.soilbio.2012.04.002

Kieft, T.L., E. Soroker, and M.K. Firestone. 1987. Microbial biomass response to a rapid increase in water potential when dry soil is wetted. Soil Biol. Biochem. 19:119–126. doi:10.1016/0038-0717(87)90070-8

Levitt, D.G., D.L. Newell, W.J. Stone, and D.S. Wykoff. 2005. Surface water–groundwater connection at the Los Alamos Canyon weir site: Part 1. Monitoring site installation and tracer tests. Vadose Zone J. 4:708–717. doi:10.2136/vzj2004.0167

Lewicki, J.L., G.E. Hilley, L. Dobeck, T.L. McLing, B.M. Kennedy, M. Bill, and B.D.V. Marino. 2013. Geologic CO_2 input into groundwater and the atmosphere, Soda Springs, ID, USA. Chem. Geol. 339:61–70. doi:10.1016/j.chemgeo.2012.06.013

Loisy, C., G. Cohen, C. Laveuf, O. Le Roux, P. Delaplace, C. Magnier, V. Rouchon, A. Cerepi, and B. Garcia. 2013. The CO_2–Vadose Project: Dynamics of the natural CO_2 in a carbonate vadose zone. Int. J. Greenh. Gas Control 14:97–112. doi:10.1016/j.ijggc.2012.12.017

Long, P.E., B. Faybishenko, T. Tokunaga, and J. Christensen. (2015). Statistical analysis of meteorological data to assess evapotranspiration and infiltration at the Rifle Site, CO, USA. In: American Geophysical Union Fall Meeting, Vol. Abstract B51C-0442. American Geophysical Union, San Francisco, CA.

Maier, M., and H. Schack-Kirchner. 2014. Using the gradient method to determine soil gas flux: A review. Agric. For. Meteorol. 192–193:78–95. doi:10.1016/j.agrformet.2014.03.006

Massman, W.J. 1998. A review of the molecular diffusivities of H_2O, CO_2, CH_4, CO, O_3, SO_2, NH_3, N_2O, NO, and NO_2 in air, O_2 and N_2 near STP. Atmos. Environ. 32:1111–1127. doi:10.1016/S1352-2310(97)00391-9

Moldrup, P., T. Olesen, J. Gamst, P. Schjonning, T. Yamaguchi, and D.E. Rolston. 2000. Predicting the gas diffusion coefficient in repacked soil: Water-induced linear reduction model. Soil Sci. Soc. Am. J. 64:1588–1594. doi:10.2136/sssaj2000.6451588x

Mosier, A.R., J.A. Morgan, J.Y. King, D. LeCain, and D.G. Milchunas. 2002. Soil-atmosphere exchange of CH_4, CO_2, NO_x, and N_2O in the Colorado shortgrass steppe under elevated CO_2. Plant Soil 240:201–211. doi:10.1023/A:1015783801324

Noe, G.B., and C.R. Hupp. 2009. Retention of riverine sediment and nutrient loads by coastal plain floodplains. Ecosystems 12:728–746. doi:10.1007/s10021-009-9253-5

Parker, L.W., J. Miller, Y. Steinberger, and W.G. Whitford. 1983. Soil respiration in a Chihuahuan Desert rangeland. Soil Biol. Biochem. 15:303–309. doi:10.1016/0038-0717(83)90075-5

Pendall, E., J.L. Heisler-White, D.G. Williams, F.A. Dijkstra, Y. Carrillo, J.A. Morgan, and D.R. LeCain. 2013. Warming reduces carbon losses from grassland exposed to elevated atmospheric carbon dioxide. PLoS One 8(8): e71921. doi:10.1371/journal.pone.0071921

Pingintha, N., M.Y. Leclerc, J.P. Beasley, G.S. Zhang, and C. Senthong. 2010. Assessment of the soil CO_2 gradient method for soil CO_2 efflux measurements: Comparison of six models in the calculation of the relative gas diffusion coefficient. Tellus B Chem. Phys. Meterol. 62:47–58. doi:10.1111/j.1600-0889.2009.00445.x

Raich, J., and W.H. Schlesinger. 1992. The global carbon dioxide flux in soil respiration and its relationship to vegetation and climate. Tellus B Chem. Phys. Meterol. 44:81–99. doi:10.1034/j.1600-0889.1992.t01-1-00001.x

Raich, J.W., and A. Tufekcioglu. 2000. Vegetation and soil respiration: Correlations and controls. Biogeochemistry 48:71–90. doi:10.1023/A:1006112000616

Rey, A. 2015. Mind the gap: Non-biological processes contributing to soil CO_2 efflux. Glob. Change Biol. 21:1752–1761. doi:10.1111/gcb.12821

Rey, A., E. Pegoraro, C. Oyonarte, A. Were, P. Escribano, and J. Raimundo. 2011. Impact of land degradation on soil respiration in a steppe (*Stipa tenacissima* L.) semi-arid ecosystem in the SE of Spain. Soil Biol. Biochem. 43:393–403. doi:10.1016/j.soilbio.2010.11.007

Rimon, Y., O. Dahan, R. Nativ, and S. Geyer. 2007. Water percolation through the deep vadose zone and groundwater recharge: Preliminary results based on a new vadose zone monitoring system. Water Resour. Res. 43. doi:10.1029/2006WR004855

Robertson, A.I., S.E. Bunn, P.I. Boon, and K.F. Walker. 1999. Sources, sinks and transformations of organic carbon in Australian floodplain rivers. Mar. Freshw. Res. 50:813–829. doi:10.1071/MF99112

Rutledge, S., D.I. Campbell, D. Baldocchi, and L.A. Schipper. 2010. Photodegradation leads to increased carbon dioxide losses from terrestrial organic matter. Glob. Change Biol. 16:3065–3074.

Salve, R. 2011. A sensor array system for profiling moisture in unsaturated rock and soil. Hydrol. Processes 25:2907–2915. doi:10.1002/hyp.8053

Scanlon, B.R., B.J. Andraski, and J. Bilskie. 2002. Miscellaneous methods for measuring matric or water potential. In: J.H. Dane and G.C. Topp, edi-

tors, Methods of soil analysis. Part 4. Physical methods. SSSA, Madison, WI. p. 643–670.

Schlesinger, W.H., and J.A. Andrews. 2000. Soil respiration and the global carbon cycle. Biogeochemistry 48:7–20. doi:10.1023/A:1006247623877

Schwesig, D., K. Kalbitz, and E. Matzner. 2003. Mineralization of dissolved organic carbon in mineral soil solution of two forest soils. J. Plant Nutr. Soil Sci. 166:585–593. doi:10.1002/jpln.200321103

Shen, Y., C.G. Fichot, and R. Benner. 2012. Floodplain influence on dissolved organic matter composition and export from the Mississippi-Atchafalaya River system to the Gulf of Mexico. Limnol. Oceanogr. 57:1149–1160. doi:10.4319/lo.2012.57.4.1149

Shroba, R.R., and R.B. Scott. 1997. Revised preliminary geologic map of the Rifle quadrangle, Garfield County, Colorado, Open File Rep. 97-852. U.S. Geological Survey, Denver, CO.

Sisson, J.B., G.W. Gee, J.M. Hubbell, W.L. Bratton, J.C. Ritter, A.L. Ward, and T.G. Caldwell. 2002. Advances in tensiometry for long-term monitoring of soil water pressures. Vadose Zone J. 1:310–315. doi:10.2136/vzj2002.3100

Tokunaga, T. 1992. The pressure response of the soil-water sampler and possibilities for simultaneous soil solution sampling and tensiometry. Soil Sci. 154:171–183. doi:10.1097/00010694-199209000-00001

Tokunaga, T.K., J. Wan, W. Dong, Y. Kim, K.H. Williams, M.E. Conrad, J.N. Christensen, M. Bill, B. Faybishenko, C. Hobson, R. Dayvault, P.E. Long, and S.S. Hubbard. 2014. Water and carbon fluxes in a semi-arid region floodplain: Multiple approaches to constrain estimates of seasonal- and depth-dependent fluxes at Rifle, Colorado. In: American Geophysical Union Fall Meeting. American Geophysical Union, San Francisco, CA.

Toosi, E.R., J.P. Schmidt, and M.J. Castellano. 2014. Land use and hydrologic flowpaths interact to affect dissolved organic matter and nitrate dynamics. Biogeochemistry 120:89–104. doi:10.1007/s10533-014-9983-0

U.S. Department of Energy. 1997. Long-term surveillance plan for the Estes Gulch Disposal Site near Rifle, Colorado. U.S. Dep. of Energy, Springfield, VA.

U.S. Department of Energy. 1999. Final site observational work plan for the UMTRA Project Old Rifle Site, Rep. No. GJO-99-88-TAR Rev. 1. U.S. Dep. of Energy, Grand Junction, CO.

van Genuchten, M.T. 1980. A closed-form equation for predicting the hydraulic conductivity of unsaturated soils. Soil Sci. Soc. Am. J. 44:892–898. doi:10.2136/sssaj1980.03615995004400050002x

Walvoord, M.A., R.G. Striegl, D.E. Prudic, and D.A. Stonestrom. 2005. CO_2 dynamics in the Amargosa Desert: Fluxes and isotopic speciation in a deep unsaturated zone. Water Resour. Res. 41: W02006.

Williams, K.H., P.E. Long, J.A. Davis, M.J. Wilkins, A.L. N'Guessan, C.I. Steefel, L. Yang, D. Newcomer, F.A. Spane, L.J. Kerkhof, L. McGuinness, R. Dayvault, and D.R. Lovley. 2011. Acetate availability and its influence on sustainable bioremediation of uranium-contaminated groundwater. Geomicrobiol. J. 28:519–539. doi:10.1080/01490451.2010.520074

Wood, B.D., C.K. Keller, and D.L. Johnstone. 1993. In situ measurement of microbial activity and controls on microbial CO_2 production in the unsaturated zone. Water Resour. Res. 29:647–659. doi:10.1029/92WR02315

Wood, C., P.G. Cook, G.A. Harrington, K. Meredith, and R. Kipfer. 2014. Factors affecting carbon-14 activity of unsaturated zone CO_2 and implications for groundwater dating. J. Hydrol. 519:465–475. doi:10.1016/j.jhydrol.2014.07.034

WRCC. 2014. Western Regional Climate Center. Desert Res. Inst., Reno, NV.

Yabusaki, S.B., Y.L. Fang, K.H. Williams, C.J. Murray, A.L. Ward, R.D. Dayvault, S.R. Waichler, D.R. Newcomer, F.A. Spane, and P.E. Long. 2011. Variably saturated flow and multicomponent biogeochemical reactive transport modeling of a uranium bioremediation field experiment. J. Contam. Hydrol. 126:271–290. doi:10.1016/j.jconhyd.2011.09.002

Zsolnay, A. 2003. Dissolved organic matter: Artefacts, definitions, and functions. Geoderma 113:187–209. doi:10.1016/S0016-7061(02)00361-0